MPPT technique based on improved evaluation of photovoltaic parameters for uniformly irradiated photovoltaic array

MPPT technique based on improved evaluation of photovoltaic parameters for uniformly irradiated photovoltaic array

A.F. Murtaza[a,*], Marcello Chiaberge[b], Filippo Spertino[c], Umar Tabrez Shami[d], Diego Boero[e], Mirko De Giuseppe[b]

[a] *Faculty of Engineering, University of Central Punjab, Lahore, Pakistan*
[b] *Department of Electronics and Telecommunication Engineering, Politecnico di Torino, Italy*
[c] *Department of Energy, Politecnico di Torino, Italy*
[d] *Department of Electrical Engineering, University of Engineering & Technology, Lahore, Pakistan*
[e] *Department of Mechanical and Aerospace Engineering, Politecnico di Torino, Italy*

A B S T R A C T

In this article, a new maximum power point tracking (MPPT) method is proposed. The proposed MPPT is in principle, a hybrid version of open circuit voltage (V_{oc}), short-circuit current (I_{sc}) and perturb & observe (P&O) techniques. Improved relations are derived in this paper on the basis of which the proposed MPPT operates. These are: voltage and current relations of PV which correspond to MPP, duty cycle function of converter to set PV operating point at MPP, criterion to measure the varying weather conditions and limits criteria to evaluate the steady weather conditions. All these relations are incorporated in the control architecture of the proposed technique, which contains three loops: E-MPP loop, R-MPP loop and S-loop. The proposed MPPT and past-proposed methods are tested through computer aided simulations and experimental prototype under dynamic and steady weather conditions. The comparative analysis between the MPPTs indicates that the proposed technique outperforms other MPPTs by a significant margin.

Keywords:
Photovoltaic (PV) systems
Maximum power point tracking (MPPT) technique
Perturb and observe (P&O)
Fractional open-circuit voltage
Weather condition evaluation

1. Introduction

Electricity generated through photovoltaic (PV) sources is expanding around the globe to meet the growing energy demands [1,2]. Under uniform weather condition, PV array exhibits the unique maximum power point (MPP) on its current–voltage (I–V) curve [3–6]. However, the MPP shifts non-linearly with changing environmental conditions like irradiance and temperature. Considering the prohibitive initial capital cost of a PV system along with its low conversion efficiency [7], it is vital to operate the PV array at MPP on a consistent basis [6]. To accomplish this, the maximum power point tracking (MPPT) technique is applied to control a DC–DC converter. A PV system architecture is shown in Fig. 1, which reveals that the major challenges in designing a MPPT are: (1) soft computing – to design an algorithm which estimates the maximum power point voltage/current (V_{mpp}/I_{mpp}) or both as its MPPT output variable, (2) hard computing – to design the converter control technique which adjusts the duty cycle of the converter to regulate the operating voltage/current (V_{pv}/I_{pv}) of PV array.

Till date, numerous MPPT techniques have been designed and some of them are surveyed by Refs. [8,9]. Many MPPT designers took the assistance from advanced control schemes like Takagi–Sugeno model based fuzzy control is used in Ref. [10] and fuzzy cognitive networks are employed with fuzzy logic control in Ref. [11]. While particle swarm optimization based MPPT is reported in Ref. [12]. These methods however, require prior tuning as well as complex optimization procedures. The surveys conducted by Refs. [8,9] reveals that perturb and observe (P&O) is the most widely used technique because of its simplicity, ease of implementation and exhibits satisfactory performance [13]. The performance of P&O is compromised under dynamically changing weather conditions, hence performance optimization methods are often applied to the basic P&O algorithm [13–15].

Several techniques have been developed to optimize the P&O method. A current based sliding control mechanism is proposed that works with an additional voltage compensation loop [16]. Similarly, a fuzzy logic control is adopted to optimize P&O in Ref. [17]. Note that the methods presented in Refs. [16,17] are complex in implementation. In Ref. [18], an adaptive perturb is calculated for

* Corresponding author.
E-mail addresses: ali.faisal@ucp.edu.pk, ali_faisal355@hotmail.com (A.F. Murtaza).

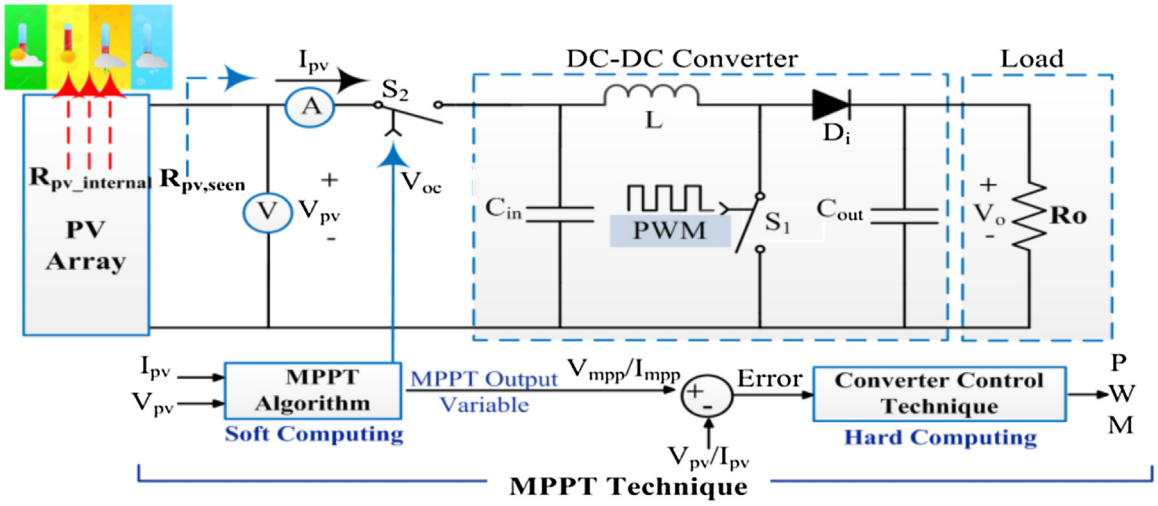

Fig. 1. Architecture of PV system in the presence of MPPT technique.

the P&O using two PI controllers, one to calculate the adaptive perturb and the other for the duty cycle of the DC–DC converter. With two PI controllers in need, this method is not cost effective.

Several MPPT techniques took the hybrid approach to enhance the performance of P&O MPPT [14,19–22]. In Ref. [19], the technique samples the open-circuit voltage (V_{oc}) and short circuit current (I_{sc}) to locate the MPP. However, the information regarding the procedure to measure V_{oc} and I_{sc} is missing. The methods presented in Refs. [14,20–22] are based on the combination of P&O and V_{oc} techniques. Techniques [20,21] measure V_{oc} to estimate the V_{mpp} but lacks a separate strategy for the estimation of duty cycle (D) of the DC–DC converter. In Ref. [22], a new relation is developed to estimate V_{oc} using temperature sensing. The use of temperature sensor adds additional cost to the system. Work presented in Ref. [14] developed two new relations for the D of the converter, and achieves better performance compared to MPPT [22]. Since the estimation of I_{sc} is achieved with moderate accuracy, this technique also utilizes PI controller to adjust D.

For grid-connected PV systems, the direct interface between the converter and inverter presents the oscillations at DC-link, which swing at double the frequency of the grid frequency [3]. Under these circumstances, the afore-mentioned PWM-based techniques require a large electrolytic capacitance at DC-link. However, it is a major source of failure in power circuits [3,16]. To enable the low non-electrolytic capacitance at DC-link; non-linear controllers based on sliding mode control (SMC) scheme have been proposed in the literature [3,16,23,24]. Methods presented in Ref. [3,16] are based on two control loops that are used to estimate the reference point and to regulate the operating point of array. In Ref. [23], a single control loop based MPPT is presented that reduces the computational complexity of the system. For stable operation, the MPPT methods presented in Refs. [3,16,23,24] must exhibit three design constraints i.e. transversality, equivalent control and reachability. Note that the design is carried out in continuous time domain and the hardware based prototype works in discrete domain; chattering occurs that can reduce the system efficiency and stability [24]. Chattering problem can only be mitigated with expensive embedded systems.

Considering these drawbacks, this paper presents a new hybrid MPPT technique, which is a combination of P&O, I_{sc} and V_{oc} techniques. The main aim is to improve the energy harvesting of PV array by enhancing the dynamic (varying weather) and steady (static weather) performances, while keeping the control algorithm simple. The salient features of the proposed MPPT are:

- V_{mpp} is estimated by measuring the V_{oc} of array with a proper clue of duration.
- A relation is developed to estimate the I_{mpp} without short-circuiting the PV array.
- Using the values of V_{mpp} and I_{mpp}, a duty cycle (D_{mpp}) relation is developed for the converter. This eliminates the need of any control schemes (PI/PID etc.)
- Frequency of V_{oc} measurement ($V_{oc,freq}$) according to varying weather condition is identified. Based on $V_{oc,freq}$, the criterion is defined with respect to sampling rate (S_R) of the PV system that decides when to measure V_{oc} according to varying weather conditions.
- Effects of steady weather conditions on PV array are evaluated under resistive and battery loads, and limits are computed.
- The control algorithm mainly contains the dynamic and steady operations. Dynamic operation is executed through two loops: E-MPP and R-MPP loops, while steady operation is accomplished through S-loop. These three loops are designed in such a manner that no power loss oscillations around MPP are produced during steady weather conditions. At the same time, the MPP tracking of the technique will be robust under varying weather conditions.

The proposed MPPT is ideally suited for stand-alone and DC-load PV systems. For grid-connected PV systems, the proposed MPPT requires a large electrolytic capacitance at the DC-link, in order to suppress the oscillations which occur due to inverter action. However, it will develop the reliability problems in the system. A more suitable grid connected PV system for the proposed MPPT is the one, where the DC–DC converter is equipped with a storage device (battery). Moreover, the proposed MPPT is not specialized in dealing with partial shading conditions.

2. Fundamental relations of the proposed MPPT technique

There are three fundamental parameters of the proposed technique: (1) V_{mpp}, (2) I_{mpp} and (3) D_{mpp}. A typical I–V curve of Kyocera 200GT module is shown in Fig. 2(a) [25], whose characteristics are: V_{oc} = 32.89 V, I_{sc} = 8.21 A, V_{mpp} = 26.3 V and I_{mpp} = 7.61 A. Fig. 2(a) indicates that the V_{mpp} and I_{mpp} can be calculated from the following two relations:

$$V_{mpp} = K_v V_{oc} \quad (1)$$

$$I_{mpp} = K_i I_{sc} \quad (2)$$

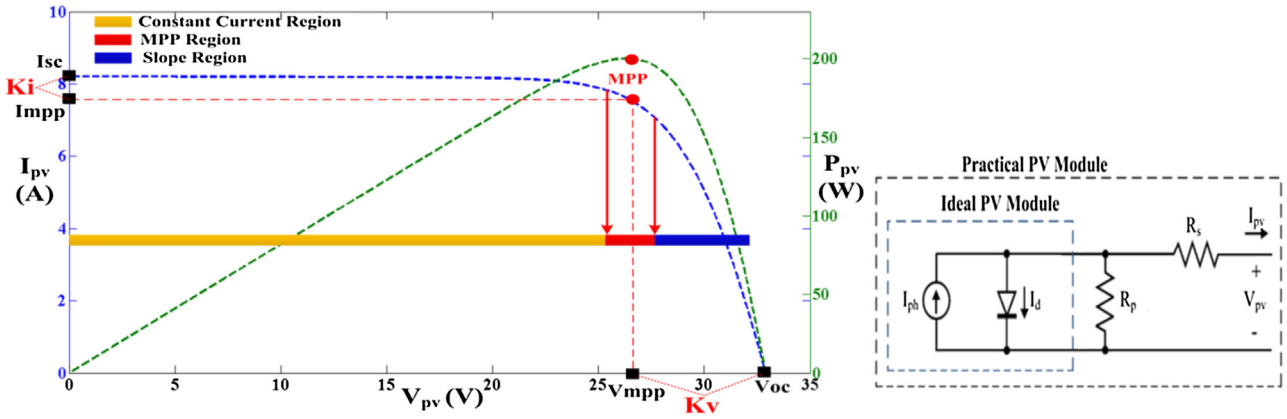

Fig. 2. (a) MPP of PV array with respect to V_{oc} and I_{sc} (left figure), (b) PV module equivalent model (right figure).

where, K_v and K_i are the proportionality constants of voltage and current respectively.

2.1. V_{mpp} calculation

For an accurate calculation of V_{mpp} through Eq. (1), the proposed technique measures the open-circuit voltage of the PV array. Since, V_{oc} measurement requires the PV array to be separated from the load, duration of V_{oc} measurement is critical. Although, PV array can be disconnected from the load using a fast switching device (S2) as shown in Fig. 1 [14,19–21]. However, the experimental evaluation of the behavior of PV array under such scenario is limited in literature.

Fig. 3 shows the experimental curves of the PV array, where it is operating at D = 90% until it is disconnected from the load at 'Arrow-1' position using a switch (n-Mosfet). It can be seen that the I_{pv} to the load immediately becomes equal to zero, while V_{pv} shoots up and executes a spike of 114.4 V. Nearly after 100 μs, V_{pv} settles down to true V_{oc} of 38 V. Since the outgoing I_{pv} is immediately terminated, PV array depicts the capacitive behavior due to its internal physics. This observation leads to two issues:

1) if V_{oc} is measured frequently, PV modules may experience a considerable stress due to these significant voltage spikes that may induce the insulation degradation of modules. However, according to IEC 61215 Standard entitled "Terrestrial photovoltaic (PV) modules—Design qualification and type approval", the PV modules under insulation test are subject to a voltage equal to 1000 V plus twice the maximum system voltage. In particular, they can tolerate up to 3000 V without insulation fault, because the maximum PV system voltage is usually equal to 1000 V. Therefore, the voltage spikes, even if remarkable, are not able to provoke a significant degradation of insulation. Also, the magnitude of voltage spikes is less at low irradiance conditions as the current generated by PV array is less. In case the voltage spikes are expected to cross these limits with large PV arrays, the switch can be relocated between the input capacitor (C_{in}) and inductor (L) of the DC–DC converter. C_{in} though increases the duration of V_{oc} measurement, nevertheless it reduces the voltage spikes as it opposes the sudden change in voltage.
2) the designer cannot measure the V_{oc} immediately and has to wait for at least 100 μs after disconnecting the PV array. To be on the safe side, the proposed method measures V_{oc} after 200 μs, whenever needed. Note that the settling time for V_{oc} depends on factors like PV array configuration, cable length and shunt/stray capacitances. Therefore, this duration can be tuned during the experimentation process.

2.2. I_{mpp} estimation

Consider the practical PV model shown in Fig. 2(b), which can be expressed in mathematical form as [26]:

$$I_{pv} = I_{ph} - I_s\left(\exp\left(\frac{V_{pv} + I_{pv}R_s}{V_T}\right) - 1\right) - \frac{V_{pv} + I_{pv}R_s}{R_p} \tag{3}$$

where, I_{ph} is the photocurrent produced by the PV array due to incident sunlight, I_s is the reverse saturation current, V_T is the thermal voltage, R_s and R_p are the equivalent series and parallel resistances of the array respectively. The information regarding the values of R_s and R_p is difficult to attain [26]. Therefore, to estimate I_{mpp}, the proposed work considers the ideal single diode model, which neglects the influence of R_s and R_p:

$$I_{pv} = I_{ph} - I_s\left(\exp\left(\frac{V_{pv}}{V_T}\right) - 1\right) \tag{4}$$

Assuming I_{ph} equals I_{sc}, the exponential factor being very large even with small forward voltage, factor '−1' can be neglected. Hence, Eq. (4) can be simplified as:

$$I_{pv} = I_{sc} - I_s\exp\left(\frac{V_{pv}}{V_T}\right) \tag{5}$$

To obtain I_s, consider PV array is operating at V_{oc}, which means that I_{pv} is equal to zero. Consequently, Eq. (5) can be re-arranged to find I_s as

$$I_s = I_{sc}\exp\left(-\frac{V_{oc}}{V_T}\right) \tag{6}$$

Putting I_s from the above relation in Eq. (5), we get:

$$I_{pv} = I_{sc}\left(1 - \exp\left(\frac{V_{pv} - V_{oc}}{V_T}\right)\right) \tag{7}$$

To calculate V_T, consider that the PV array is operating at MPP i.e. $I_{pv} = I_{mpp}$ and $V_{pv} = V_{mpp}$, therefore the above equation can be re-arranged as:

$$V_T = \frac{V_{mpp} - V_{oc}}{\ln\left(1 - \frac{I_{mpp}}{I_{sc}}\right)} \tag{8}$$

Putting the value of V_T from the above relation in Eq. (7), we get

$$I_{pv} = I_{sc}\left(1 - \exp\left(\frac{\left(V_{pv} - V_{oc}\right) \times \ln\left(1 - \frac{I_{mpp}}{I_{sc}}\right)}{V_{mpp} - V_{oc}}\right)\right) \tag{9}$$

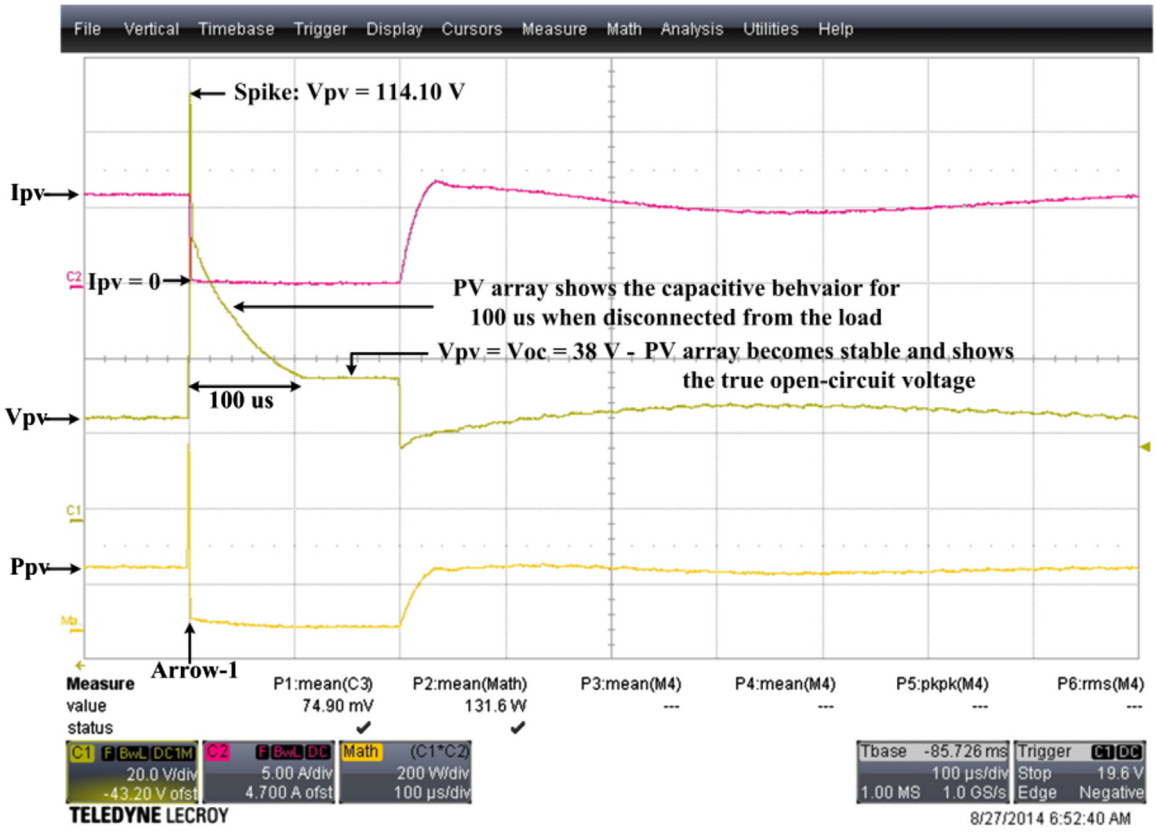

Fig. 3. Experimental test of duration of V_{oc} measurement.

We know that $V_{mpp} = K_v V_{oc}$, $I_{mpp} = K_i I_{sc}$ and $I_{sc} = I_{mpp}/K_i$, therefore putting these relations in the above relation, I_{mpp} can be found out as:

$$I_{mpp} = \frac{K_i I_{pv}}{1 - \exp\left(\frac{(V_{pv} - V_{oc}) \times \ln(1-K_i)}{V_{oc}(K_v - 1)}\right)} \tag{10}$$

2.3. D_{mpp} estimation

Impedance relation of boost converter can be written as [14]:

$$R_L = \frac{1}{(1-D)^2} R_{pv\_seen} \rightarrow R_L = \frac{1}{(1-D)^2} \frac{V_{pv}}{I_{pv}} @Non - MPP \tag{11}$$

$$R_L = \frac{1}{(1-D)^2} R_{pv\_seen} \rightarrow R_L = \frac{1}{(1-D_{mpp})^2} \frac{V_{mpp}}{I_{mpp}} @MPP \tag{12}$$

In the above relation, R_{pv_seen} is the impedance seen by the PV module. At MPP, R_{pv_seen} becomes equal to V_{mpp}/I_{mpp}, which matches the load resistance (R_L) at $D = D_{mpp}$. Assuming the R_L to be constant [14], Eqs. (11) and (12) can be equated to find D_{mpp} as:

$$D_{mpp} = 1 - \left((1-D) \times \sqrt{\frac{V_{mpp} I_{pv}}{V_{pv} I_{mpp}}}\right) \tag{13}$$

where, D_{mpp} is the duty cycle for the next iteration, while D is the current duty cycle. It can be noticed that when PV array starts operating at MPP i.e. $V_{mpp} \approx V_{pv}$ and $I_{mpp} \approx I_{pv}$, Eq. (13) is transformed into the form $D_{mpp} = D$. Putting I_{mpp} from Eq. (10) and V_{mpp} from Eq. (1) in Eq. (13), we get

$$D_{mpp} = 1 - \left((1-D) \times \sqrt{\frac{K_v V_{oc}\left(1 - \exp\left(\frac{(V_{pv} - V_{oc})\ln(1-K_i)}{V_{oc}(K_v - 1)}\right)\right)}{K_i V_{pv}}}\right) \tag{14}$$

The above equation depicts the optimum duty cycle relation of the proposed technique. The above relation is valid only for boost topology, however a procedure described in Section 2.3 can be followed to find the D-relation of other converters.

3. Evaluation of weather conditions by the proposed MPPT

The proposed MPPT evaluates the weather conditions in distinct way during its dynamic operation as compared to its steady operation.

3.1. Weather evaluation during dynamic operation

During the search of MPP point, the technique takes an idea about the ambient condition by measuring the V_{oc} value. Since V_{oc} measurement is a power loss, the frequency of V_{oc} measurement ($V_{oc,freq}$) is critical, especially when PV array is under fast varying weather conditions. It has been reported by Refs. [4,27] that the rate of change of weather conditions cannot be faster than 100 ms (0.1 s). Therefore, the $V_{oc,freq}$ is set at 100 ms. After every 100 ms, the technique measures V_{oc} value regardless of weather conditions. Furthermore, considering the 0.2 ms ($V_{oc,meas}$ = 200 µs) loss of power per 100 ms ($V_{oc,freq}$ = 100 ms) during fast varying conditions, the advantage expected to be gained by closing the gap to

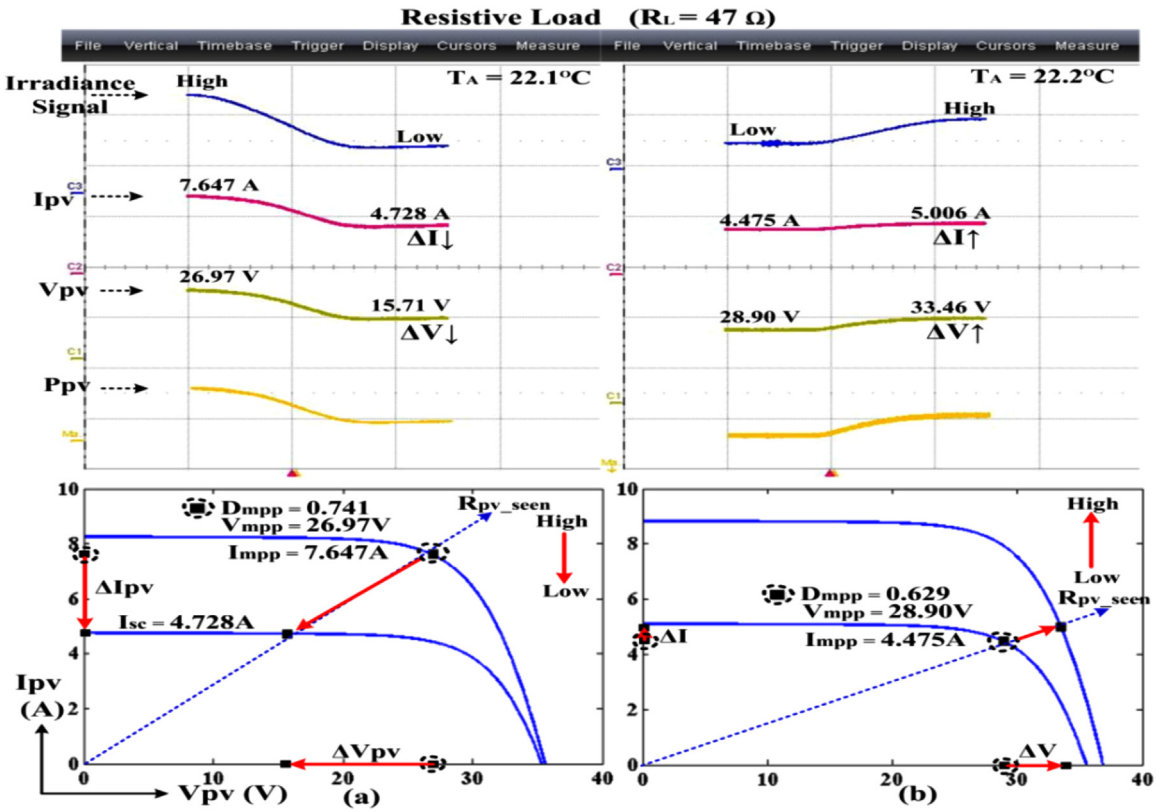

Fig. 4. Experimental tests to evaluate varying weather under resistive load.

the MPP not only covers the loss power of 0.2 ms but also gives the improved efficiency.

3.2. Weather evaluation during steady operation

Once proposed MPPT attains the MPP point, its steady operation is started. During this operation, the weather conditions (static/changed) are evaluated without measuring the V_{oc} value. For this reason, the technique sets the limit criteria for I_{pv} and V_{pv} such that if PV array violates these limits, MPPT algorithm terms this as a change in weather condition and restart the dynamic operation. The value of these limits is calculated experimentally using two loads: (1) resistive load of 47 Ω and (2) battery of 49.1 V. Details of experimental setup are mentioned in Section 6.

3.2.1. Resistive load (47 Ω)

Upper graphs of Fig. 4 show the captured oscilloscope waveforms for I_{pv} and V_{pv}. These oscilloscope plots are retrofitted in terms of the I–V curves for better understanding in lower graphs. Lower graph of Fig. 4(a) shows that D_{mpp} is initially set at 0.741 to operate the array at V_{mpp} = 26.97 V. After that, the irradiance level changes from high to low level, while PV array is operating with the same D_{mpp} = 0.741. Consequently, the PV array follows the load line and starts operating in constant current region, which in turn, brings a notable change in V_{pv} and I_{pv} of the array. On the other hand, Fig. 4(b) shows that in order to operate the PV array at V_{mpp} = 28.90 V when irradiance is low, D_{mpp} is configured at 0.629 (62.9%). And when the condition changes from low to high, the PV array once again follows the load line and starts operating in slope region. This brings a significant change in V_{pv} and marginal change in I_{pv}. From these observations, it can be concluded that while operating at MPP with same D_{mpp} against resistive load, if there will be a change in weather conditions, V_{pv} will change significantly.

3.2.2. Battery load (49.1 V)

Fig. 5 shows the response of the PV array while moving from high to low irradiance levels and vice-versa under the battery load. In first case as shown in Fig. 5(a), D_{mpp} is set at 0.494 (49.4%) to settle the array at V_{mpp} = 27.21 V. When condition changes from high irradiance to low irradiance, while PV is operating with same D_{mpp}, the array follows the battery load line and falls relatively in the same region. This brings a significant change in I_{pv}, while change in V_{pv} is almost negligible [28]. Same is the case while going from low irradiance to high irradiance as shown in Fig. 5(b). Note that battery offers very low resistance, hence the battery load-line is virtually straight. All these conditions can be summarized as:

- Resistive Load (High to Low Irradiance): $\Delta V_{pv}\downarrow$ (significant) and $\Delta I_{pv}\downarrow$ (significant).
- Resistive Load (Low to High Irradiance): $\Delta V_{pv}\uparrow$ (significant) and $\Delta I_{pv}\uparrow$ (marginal).
- Battery Load (High to Low Irradiance): $\Delta V_{pv}\approx$ (same) and $\Delta I_{pv}\downarrow$ (significant).
- Battery Load (Low to High Irradiance): $\Delta V_{pv}\approx$ (same) and $\Delta I_{pv}\uparrow$ (significant).

It is deduced that with a constant voltage load, only ΔI_{pv} is enough to evaluate the weather conditions. On the other hand, ΔV_{pv} gains importance while working with resistive load.

3.2.3. ΔI_{lim} criteria

For the proposed technique, in order to remain in the steady operation i.e. to hold the MPP point, the following condition should be satisfied:

$$|I_{mpp} - I_{pv}| \leq \Delta I_{lim} \tag{15}$$

where, I_{pv} is current value at the present instant and ΔI_{lim} is the threshold limit of I_{pv}. Normally the threshold limit for I_{pv} (ΔI_{lim}) is

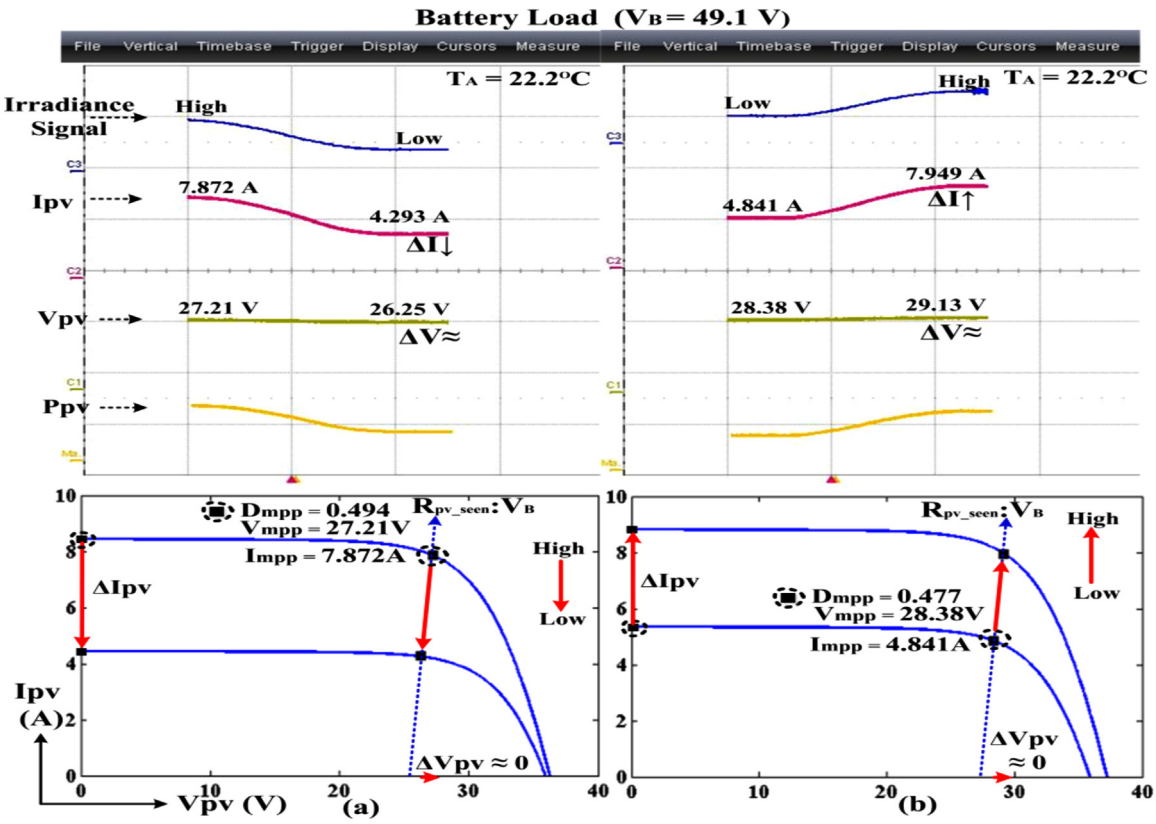

Fig. 5. Experimental tests to evaluate varying weather under battery load.

selected with respect to the I_{pv} (STC) of PV array. Technique [19] set the ΔI_{lim} as 1% of I_{pv} (STC). However, considering the measuring tolerance of the sensor and noise disturbances present in the system [29], the magnitude of ΔI_{lim} should not be too small. Otherwise, the PV array cannot differentiate between the two scenarios: (1) ΔI_{lim} is violated because of the noise/sensing error of the PV system or (2) due to the change in weather conditions. Consequently, the steady efficiency of the technique will be compromised. For instance, PV array has I_{pv} (STC) = 10 A, then with 1% of limit [19], ΔI_{lim} will be 0.1 A which is too low.

On the other hand, if the ΔI_{lim} is set too high then the PV array stays in steady operation for longer period and even may not break the ΔI_{lim} for notable change in irradiance. Due to which the dynamic efficiency of the technique suffers. Considering these facts, the proposed technique sets the ΔI_{lim} when there is a change in irradiance of atleast 20 W/m^2 which can be calculated as:

$$\Delta I_{lim} = I_{pv,stc} - \left(I_{pv,stc} \times \left(\frac{980 W/m^2}{1000 W/m^2} \right) \right) \tag{16}$$

3.2.4. ΔV_{lim} criteria

The proposed technique utilizes the voltage steps (ΔV) in its operation, the working of which is explained in the next section. Hence, threshold limit of V_{pv} (ΔV_{lim}) of the technique is fairly easy to set i.e.

$$\Delta V_{lim} = \Delta V \tag{17}$$

$$|V_{mpp} - V_{pv}| \leq \Delta V_{lim} \tag{18}$$

It should be noted that the proposed MPPT enters in steady operation when MPP is attained, the technique stores the I_{mpp} and V_{mpp} values. During steady operation, the technique keeps on sampling the I_{pv} and V_{pv} values, and evaluates the limit conditions to decide whether to stay in steady operation or move back to dynamic operation.

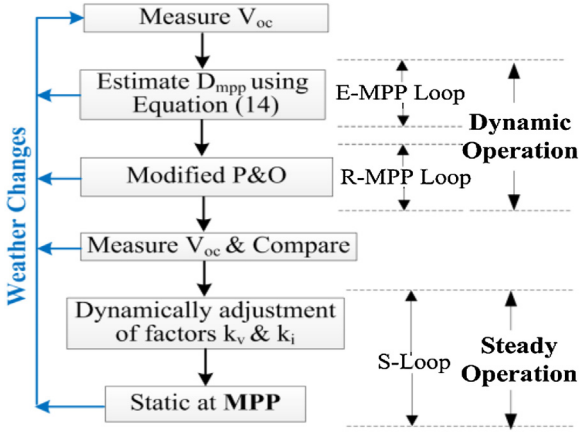

Fig. 6. Basic outline of the proposed MPPT.

4. Control algorithm of the proposed MPPT technique

4.1. Brief overview of the control algorithm

The control algorithm of the proposed technique revolves around dynamic and steady operations. Fig. 6 illustrates that dynamic operation contains two loops, which are E-MPP and R-MPP loops. While steady operation possesses only S-loop. E-MPP loop is the estimated-MPP loop and is responsible to set the V_{pv} of PV array near MPP vicinity through D_{mpp} relation expressed in Eq. (14). Since D_{mpp} relation has been developed from I_{mpp} and V_{mpp} estimations, it may not set the PV array at MPP precisely. The second loop is the

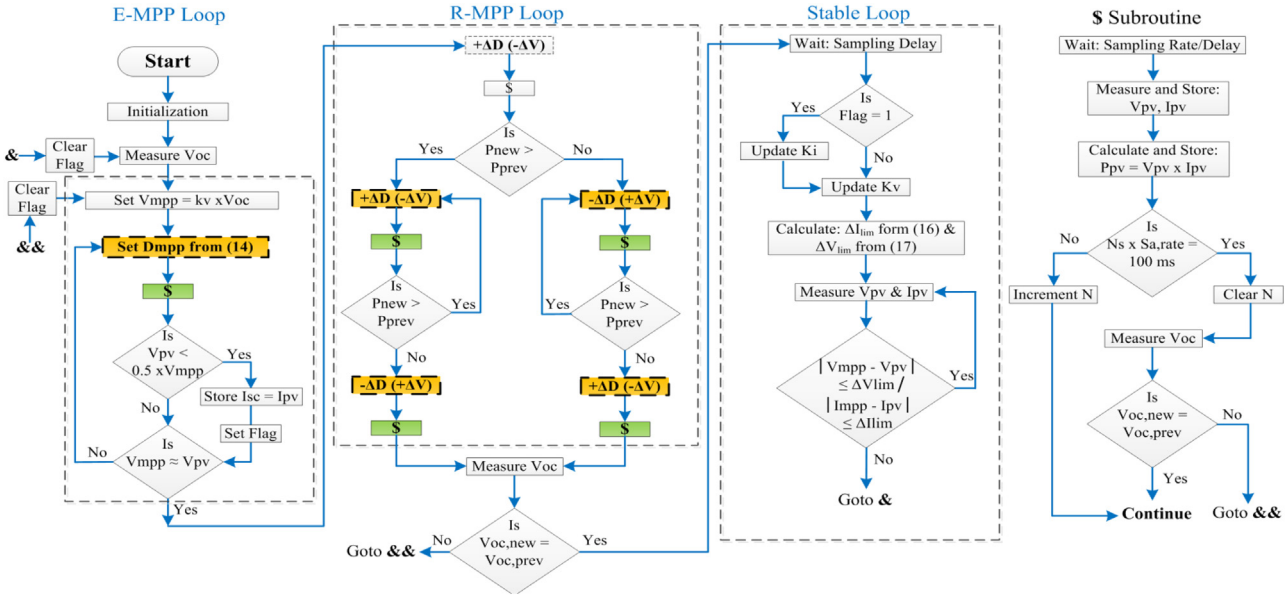

Fig. 7. Operational flowchart of the proposed technique.

real-MPP loop i.e. R-MPP loop. It contains the modified P&O algorithm that tunes the D_{mpp} further to set the PV array at exact MPP. Finally, the algorithm proceeds to S-loop known as the stable-loop i.e. steady operation. Since the algorithm enters in this loop while PV array is operating at MPP, the algorithm imposes the limits criteria in this loop. The ΔI_{lim} and ΔV_{lim} limits can be calculated from Eqs. (16) and (17) respectively, which are as described in the previous section. The proposed method remains in S-loop until the limits are violated. In case of violation of limits, the algorithm returns back to E-MPP loop and the dynamic operation is re-initiated. Note that during dynamic operation i.e. in E-MPP/R-MPP loops, the proposed MPPT measures the V_{oc} value by disconnecting the array from the load at a frequency of 100 ms. If the two consecutive V_{oc} values differ from each other, it indicates the change in weather conditions. Consequently, the proposed MPPT re-starts the dynamic operation.

4.2. Detailed architecture of the control algorithm

Fig. 7 illustrates the working flowchart of each stage. The algorithm starts the process by initializing the values of D_{in}, K_i, K_v. Where, initial values of K_i and K_v can be calculated using Eqs. (19) and (20) respectively from STC data, which is available in the manufacturer's datasheet:

$$K_i = \frac{I_{mpp}\,(STC)}{I_{sc}\,(STC)} \tag{19}$$

$$K_v = \frac{V_{mpp}\,(STC)}{V_{oc}\,(STC)} \tag{20}$$

Flowcharts of first two stages i.e. E-MPP and R-MPP loops indicate that the duty cycle blocks (dotted lines) are always followed by special '$' block stage. The working of this block is shown on right side of the flowchart. Whenever algorithm enters in this '$' block after computing D, the designer has to wait for sampling rate (S_R) before sensing the V_{pv}/I_{pv} values. The sampling rate, normally varies from 5 ms to 50 ms depending upon the PV system [15], is essential to ensure that the PV array has reached the steady state after every perturbation in D [14,15,30]. Any control decision taken during the transient period may mislead the MPPT algorithm [30].

The soft computing calculations like duty cycle relation from Eq. (14) can be executed merely in microseconds with the fast processing devices of current era. However, the MPPT designer has to wait for the S_R (milliseconds) after every change in D. Neglecting the processing time of the digital device, the time response (T_r) of the technique can be formulated with respect to the number of samples (N_s) required to tune D in order to set PV array at MPP can be expressed in Eq. (21) as

$$T_r = N_s \times S_R \tag{21}$$

Another thing which can be noticed in '$' block is when to measure the V_{oc} value to judge the varying weather conditions. Since the $V_{oc,freq}$ is set at 100 ms, the above equation is also used to determine the sample at which V_{oc} will be measured i.e.

$$N_{voc} : N_s \times S_R = 100\text{ms} \tag{22}$$

Consider that S_R is 10 ms, the algorithm measures V_{oc} at every tenth sample.

4.2.1. E-MPP loop

Fig. 7 shows that before entering into E-MPP loop, the algorithm measures $V_{oc,}$ which is required to calculate the D_{mpp} value from Eq. (14) and also reference voltage V_{mpp}. After every duty cycle computation, the algorithm first checks the condition that V_{pv} is less than $0.5 \times V_{mpp}$ i.e. 50% of V_{mpp}. If it is true, it means that the PV array is operating in constant current region, where $I_{pv} \approx I_{sc}$. Hence, the value of I_{sc} is stored and flag is set such that the value of K_i (which requires I_{mpp} and I_{sc}) can be updated later when MPP is reached. After that, algorithm checks the condition that V_{pv} is equal to V_{mpp}. Whenever this condition becomes true, algorithm proceeds to R-MPP loop.

4.2.2. R-MPP loop

It is expected that the technique brings V_{pv} of the array near MPP region when it leaves the E-MPP loop. R-MPP loop is a modified P&O loop, which sets the V_{pv} of PV array to real MPP by fine tuning the D_{mpp}. The working principle of this loop is shown in Fig. 7, while its execution is shown in Fig. 8. The first step ($-\Delta V$) of this loop will decide the direction in which the real MPP is present. If P_{new} is greater, it means that MPP is present in the same direction as shown in Fig. 8 and algorithm proceeds with the same $-\Delta V$ steps. The flowchart in Fig. 7 further shows that the last step of R-MPP loop is opposite to the direction in which it is proceeding. This mechanism can be judged from Fig. 8 that after reaching the MPP

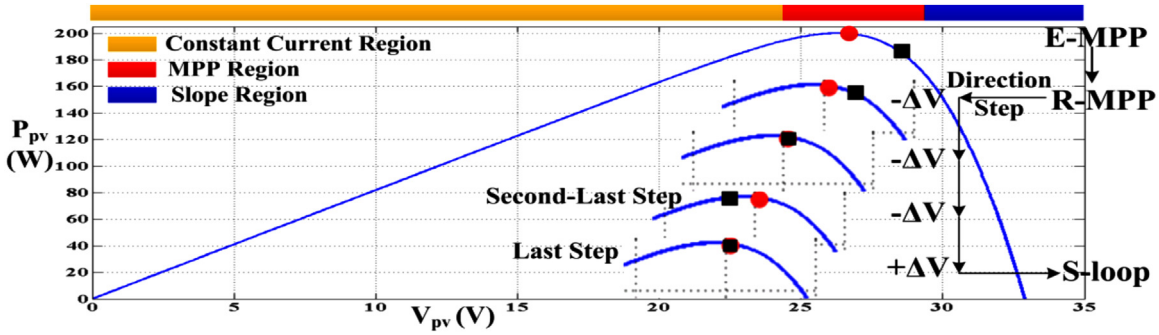

Fig. 8. Detection of MPP precisely.

by taking $-\Delta V$ steps, the algorithm crosses the MPP with another $-\Delta V$ step i.e. second-last step. Consequently, P_{new} is less than P_{prev}, therefore the algorithm returns back to MPP with $+\Delta V$ (opposite to the direction), which is the last step of R-MPP loop and proceeds to the S-loop. It should be noted that during R-MPP loop, the algorithm always contains the information of V_{oc} via '$' blocks. Whenever, it finds out that V_{oc} is changed, it will return to E-MPP loop with the help of '$' block instead of going into S-loop.

4.2.3. S-loop

Fig. 7 shows that the algorithm measures the V_{oc} again before moving to S-loop to assess the weather conditions. Since the algorithm enters in S-loop while operating at MPP accurately, the algorithm has the accurate data of V_{mpp} and I_{mpp} along with V_{oc} and I_{sc} (if flag is set in E-MPP loop). Hence, the algorithm always updates the K_v value (ratio of V_{mpp}/V_{oc}) while K_i value (ratio of I_{mpp}/I_{sc}) is updated based on the flag status. The flag is set only when PV array somehow moves in constant current region as already explained in E-MPP loop. After that, the algorithm calculates the ΔV_{lim} and ΔI_{lim} from Eqs. (16) and (17) respectively and continuously monitors the two conditions. Whenever, either of the limit is crossed, the technique will return back to E-MPP loop to re-initiate the process.

Note that the proposed technique is designed for uniform weather conditions, whereas its performance degrades under partial shading conditions. Since, the proposed MPPT always sets the PV array at a voltage determined by relation K_vV_{oc}, the proposed MPPT tracks the global maximum (GM) when it occurs in the same region. However, if GM occurs far away from K_vV_{oc}, the proposed MPPT will get caught in the local maximum.

5. Simulation results and comparative study

The capabilities of four MPPTs are assessed by executing them in Matlab/Simulink using the PV system framework as shown in Fig. 1. These MPPTs are: proposed MPPT, sliding-mode controller based MPPT (Sliding [3]), duty-cycle based MPPT (MPPT [31]) and classical P&O. Boost topology is selected whose components values for Sliding [3] are $C_{in} = 90\ \mu F$, $L = 30\ \mu F$ & $C_{out} = 90\ \mu F$. While, the values of the converter components for other three MPPTs are $C_{in} = 50\ \mu F$, $L = 300\ \mu F$ & $C_{out} = 100\ \mu F$. To ensure the smooth operation and fast sampling rate ($S_R = 1$ ms) of Sliding [3], the components values of converter are made distinctive. While, other techniques work with a switching frequency of 70 kHz and decisions are updated after every 2 ms. To execute the voltage steps, ΔD of proposed method, MPPT [31] and classical P&O is settled at 0.015. While, the parameters of admittance formula for Sliding [3] are configured to execute $\Delta V = 1.5$ V.

The first test involves the step rise of weather condition from $500\ W/m^2$ – 20 °C to $1000\ W/m^2$ – 25 °C. Initially, all MPPTs are configured to operate at MPP and then the conditions are changed to higher levels at 4 ms as shown in Fig. 9. Due to resistive load, the operating points of all MPPTs move to slope region. Fig. 9 indicates that the proposed MPPT measures the V_{oc} value when condition changes and MPP is tracked within 16 ms. In the process, the proposed method takes six control decisions and 12 ms, as $S_R = 2$ ms, to reach the optimal point. Sliding [3] also achieves the MPP point within 16 ms and for that, it executes 13 perturbations similar to that of P&O but with less voltage ripples. Due to fast $S_R = 1$ ms, the tracking time of Sliding [3] is similar to the proposed MPPT. However, during the MPP search, the proposed method through its D relation, as expressed in Eq. (14), quickly adjusts the V_{pv} of array near MPP point. While Sliding [3] gradually reaches the MPP region. The resulting V_{pv} profile of each technique is shown in lower graph of Fig. 9. It can be seen that the proposed MPPT always operates near V_{mpp} compared to other MPPTs during MPP search. Hence, the proposed method has the superior dynamic efficiency.

MPPT [31] exhibits inferior performance compared to proposed MPPT and Sliding [3] as it reaches the optimal point at 24 ms. The major downside of this MPPT is that when it falls in a slope region, its I_{mpp} and V_{mpp} estimations are relatively weak. P&O has the most degraded performance as it reaches the MPP point at 30 ms. The steady state efficiencies of MPPTs are also evaluated from 30 ms to 42 ms. A zoomed view of steady response of each MPPT is shown in right-top side of Fig. 9. Both Sliding [3] and P&O execute steady state oscillations around MPP, while proposed MPPT does not produce these steady oscillations. The dynamic and steady-state efficiencies of MPPTs are mentioned in Table 1 under each case.

Fig. 10 presents the performance of MPPTs when weather parameters are varied from $1000\ W/m^2$ – 25 °C to $750\ W/m^2$ – 22 °C. As a result, the operating points of techniques move from MPP region to constant current region. Under the present scenario, the tracking ability of MPPTs is: proposed MPPT = 14 ms, Sliding [3] = 15 ms, MPPT [31] = 16 ms and P&O = 16 ms. As clearly seen in Fig. 10 the proposed MPPT outperforms the benchmark techniques. Thus justifying the D relation and working principle of the proposed method. Contrary to previous case, the performance of the MPPT [31] is not only close to proposed MPPT, but it also extracts more power than Sliding [3] during MPP search. It is because of the reason that when PV array falls in constant current region, MPPT [31] utilizes the better estimation through $I_{mpp} = 0.8\ I_{sc}$ relation.

The last case is the variation of load from 25 Ω to 40 Ω under STC. All MPPTs are first settled at MPP under 25 Ω and then the load changes from 25 to 40 Ω at 4 ms as shown in Fig. 11. In this case, Sliding [3] has the best response and it achieves the MPP point within two samples as presented in Fig. 11. Note that when load changes, the operating point of MPPTs moves from MPP to slope region. Since, the proposed MPPT takes the load variations as change in weather conditions, it executes similar procedure as that of case-1 and consumes few samples to reach the MPP. Nevertheless, the proposed MPPT outperforms the MPPT [31] and P&O, while its performance is close to Sliding [3].

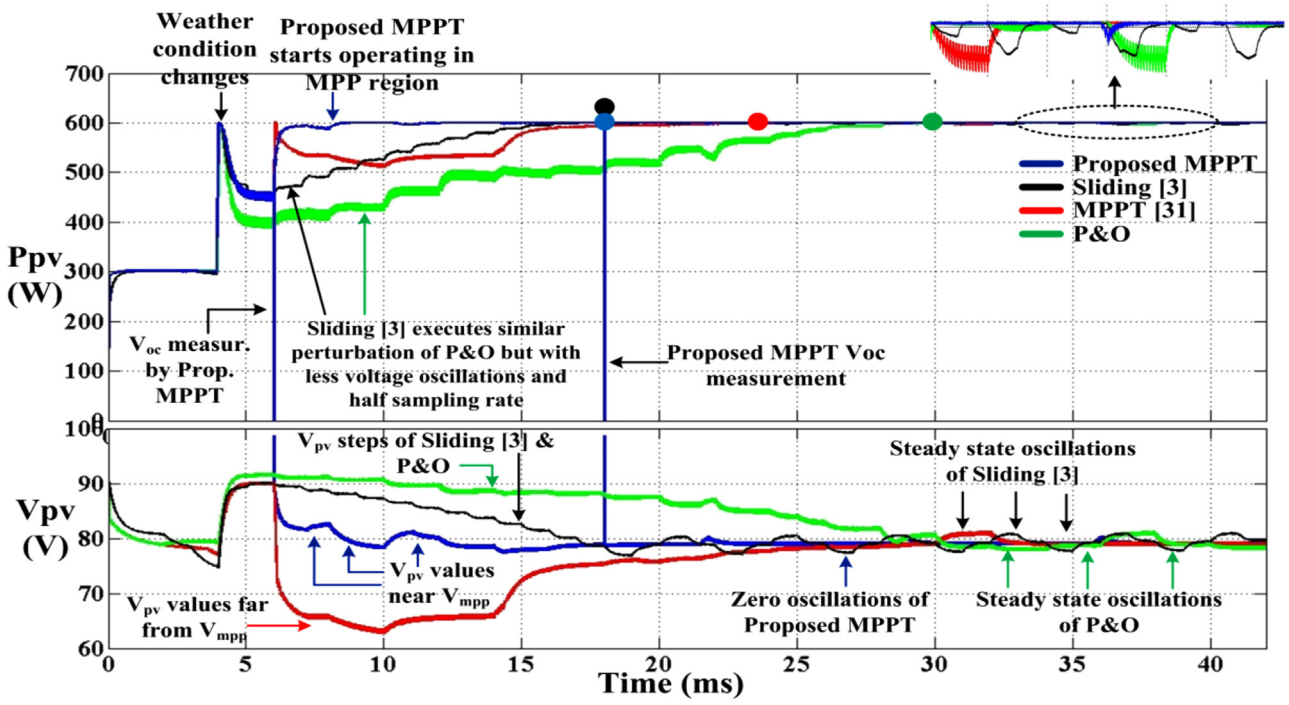

Fig. 9. P_{pv} and V_{pv} curves of MPPTs against step rise in weather condition.

Table 1
Dynamic and steady state efficiencies of MPPTs.

Conditions	Tracking ability (ms)				Efficiencies attained by MPPTs (%)				
	Proposed MPPT	Sliding [3]	MPPT [31]	P&O	Measurement period (ms)	Proposed MPPT	Sliding [3]	MPPT [31]	P&O
Rising weather	12 ms	13 ms	18 ms	24 ms	6 ms–30 ms	99.71	95.82	95.55	85.97
Falling weather	8 ms	10 ms	10 ms	10 ms	6 ms–16 ms	99.21	94.87	98.92	94.49
Load variation	10 ms	2 ms	14 ms	16 ms	6 ms–22 ms	99.78	99.85	99.18	95.42
Steady weather	–	–	–	–	30 ms–42 ms	≈100	≈99.9	≈100	≈99.9

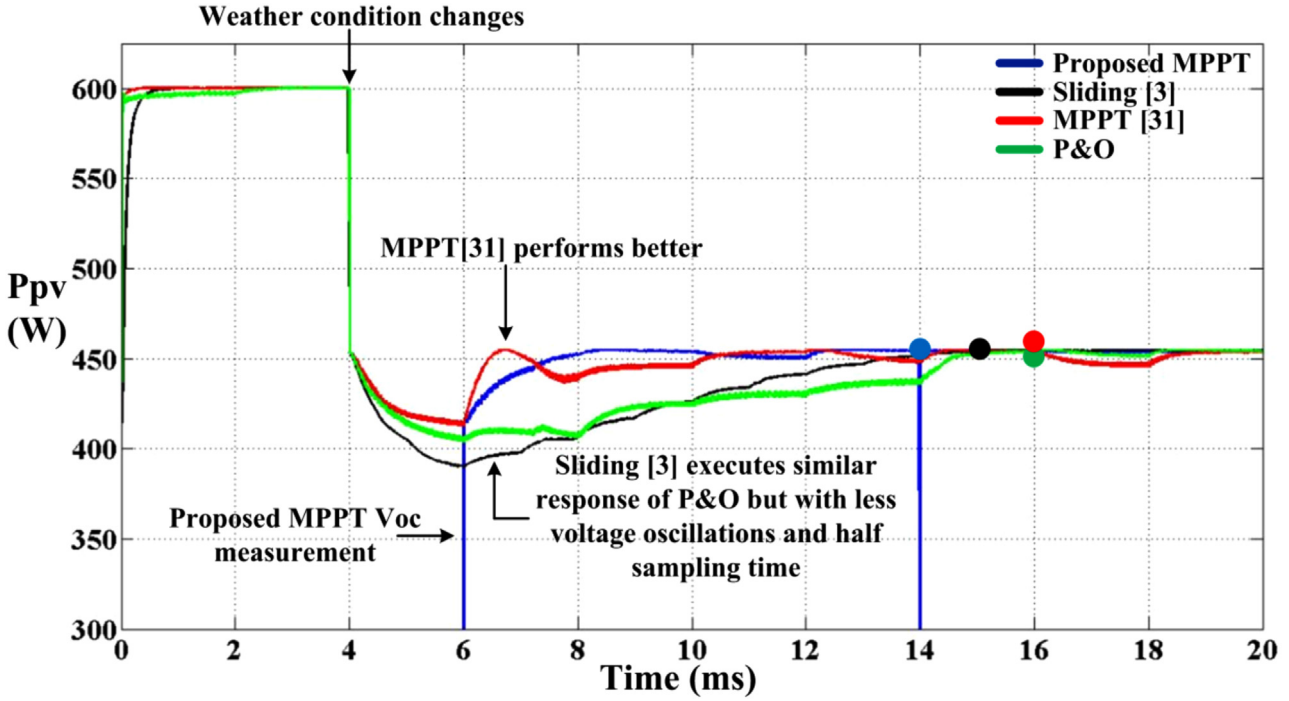

Fig. 10. Response of MPPTs against step fall in weather condition.

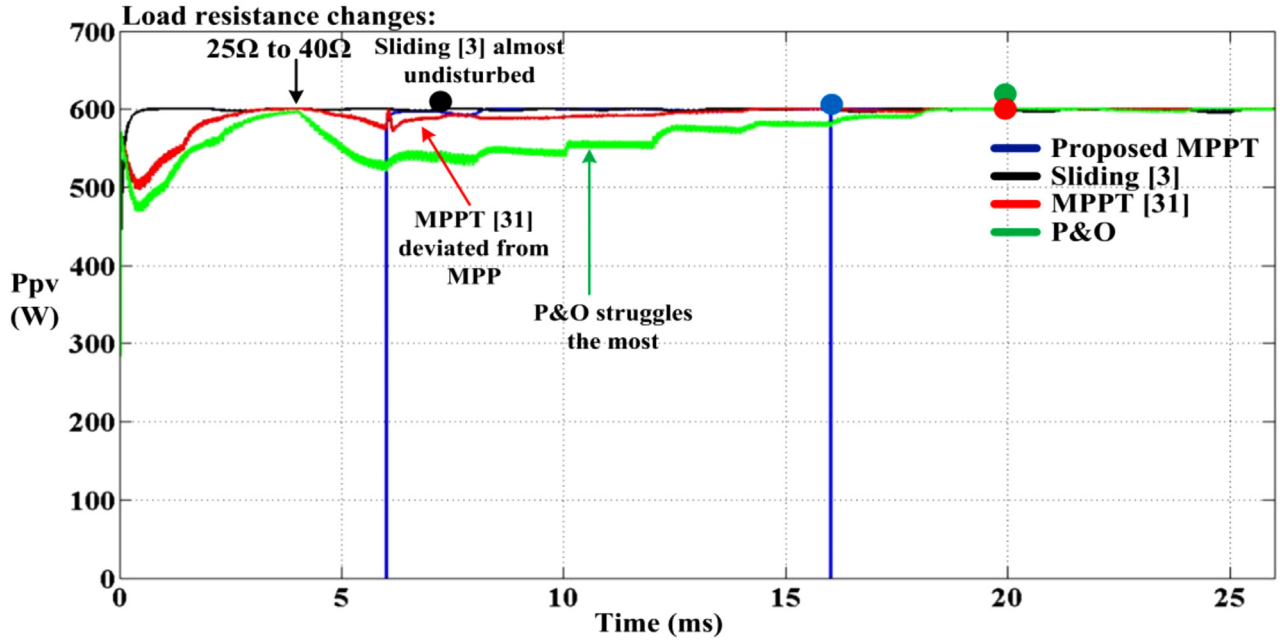

Fig. 11. Performance of MPPTs against load variation.

Table 1 summarizes the above mentioned simulation results, which indicate that proposed MPPT is the only technique, which guarantees more than 99% of efficiency under each case.

5.1. Implementation cost and embedded system

Table 2 presents the setup requirement for each MPPT along with the implementation cost. It can be seen that P&O has the lowest investment, as it requires an inexpensive embedded system along with two sensors (I_{pv} and V_{pv}). Since other three MPPTs execute complex computations in their operations, they require advanced processing unit. However, considering the power deficit of P&O compared to other MPPTs as shown in Table 1, the additional cost of other three MPPTs can be recovered in a short-period of time. Amongst the three latest MPPTs, Sliding [3] is the most expensive one as it requires sophisticated data-acquisition system and high processing speed in order to minimize the chattering effects. Moreover, it utilizes a Salman-Key filter to measure I_{pv} from I_L current sensor. Although proposed MPPT requires an extra switch to measure the V_{oc} value compared to MPPT [31], the high-resolution data acquisition demand of MPPT [31] balances out the implementation cost of the two MPPT.

6. Experimental validation

To assess the performances of MPPTs, the experimental apparatus shown in Fig. 12 has been utilized. Individual devices of experimental setup are mentioned with labels in Fig. 12. A PV array is mounted on a special mobile vehicle to conduct the dynamic tests. The irradiance meter is mainly exercised to realize the state of weather condition. However, to detect the ideal MPP during each test, the P–V curve is initially scanned for 10 ms with 1 mF capacitor. Boost converter is used, whose components values are: C_{in} = 150 uF, L = 200 uH, C_{out} = 250 uF. Switching frequency of boost converter is set at 40 kHz. Responses of proposed MPPT and P&O are collected under various weather conditions against two different loads i.e. resistive (47 Ω) and battery (49.1 V). Both techniques are assigned with a $\Delta D = 0.03$ to execute the voltage steps. Sampling rate (S_R) of each technique is set at 10 ms. Since the proposed technique requires V_{oc} in its operation, it measures the V_{oc} value after every 100 ms ($V_{oc,freq}$ = 100 ms) and 200 μs are consumed to obtain the V_{oc} value.

6.1. Time response analyses of techniques

6.1.1. Resistive load (47 Ω)

All the experimental tests conducted in this section contain the same format as shown in Fig. 13, which is: (1) I–V curve is scanned for 10 ms to attain the ideal MPP, (2) initial duty cycle (D_{in}) is set at 0.9 (90%) and (3) operation of the technique starts. For fair comparison, the tests are conducted under similar weather conditions. Figs. 13(a) and 13(b) show the performances of the proposed technique and P&O respectively. Since the weather conditions exhibit the I_{sc} of 9.93 A (for proposed MPPT) and 9.81 A (for P&O), which are greater than I_{sc} (STC) = 8.8 A, conditions are declared as high irradiance. As shown in Fig. 13(a) after D_{in} = 0.9, the technique measures V_{oc} before entering into E-MPP loop where it takes 2 samples. After that, the technique enters into R-MPP loop where it utilizes 3 samples to reach MPP. In total, the proposed technique utilizes 5 samples to attain the optimal point. Finally, it measures the V_{oc} again to assess the weather conditions. Since weather is not changed as confirmed by the irradiance signal, the proposed technique enters into S-loop where it is stable and executes negligible power loss oscillations. On the other hand, P&O takes 9 samples to reach MPP and after that it starts producing power loss oscillations around MPP.

Fig. 14 shows the response of two techniques when the weather is at medium irradiance level. Under present weather condition, the proposed MPPT consumes 6 samples to attain the MPP. However, P&O needs 14 samples to reach MPP. On the other hand, Fig. 15 gives an idea about the performances of the techniques at low irradiance. Once again, P&O performance degrades further and executes 18 samples to reach MPP while the performance of proposed MPPT remains intact and takes 5 samples to attain the optimal point.

The reason behind the degradation of P&O performance under resistive load, while moving from high to low irradiance condition, can be evaluated with the help of Table 3, where all these tests are summarized. It can be noticed under P&O section, although the V_{mpp} values of different conditions are close but D_{mpp} values to operate the PV array at these V_{mpp} values are vastly different. For instance, the difference in D_{mpp} values between high and low

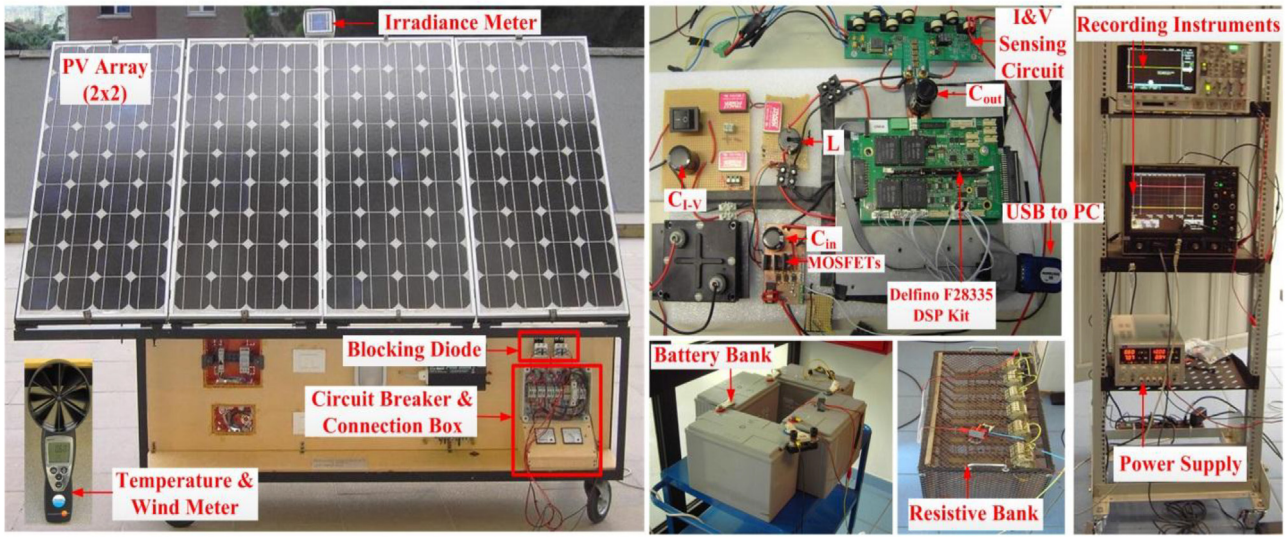

Fig. 12. Experimental apparatus with mobile PV array.

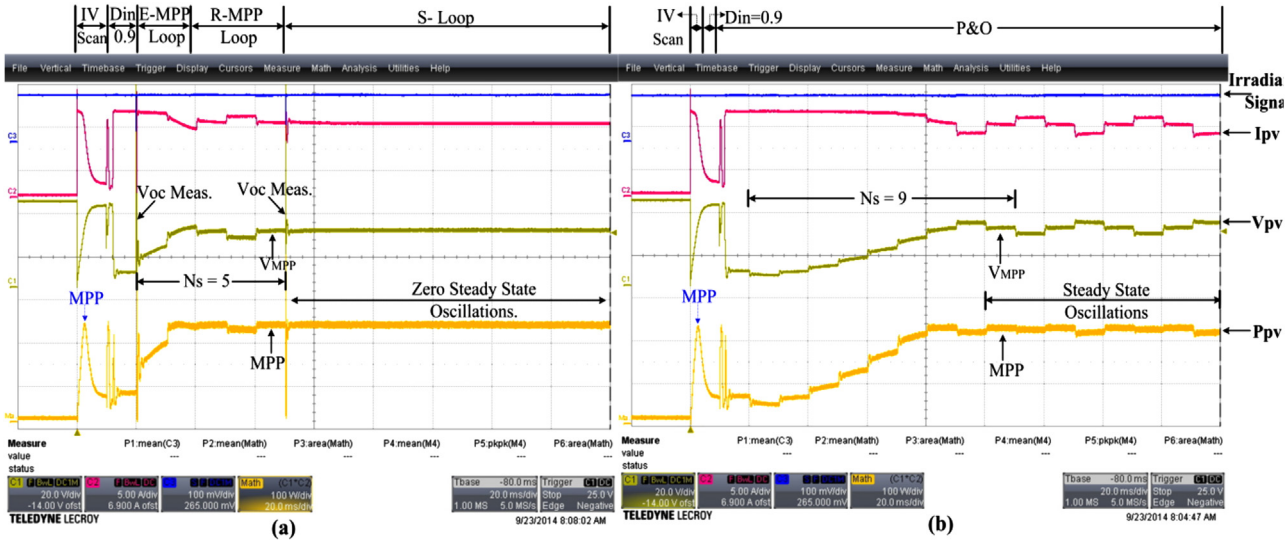

Fig. 13. Response of techniques at high irradiance against resistive load technique.

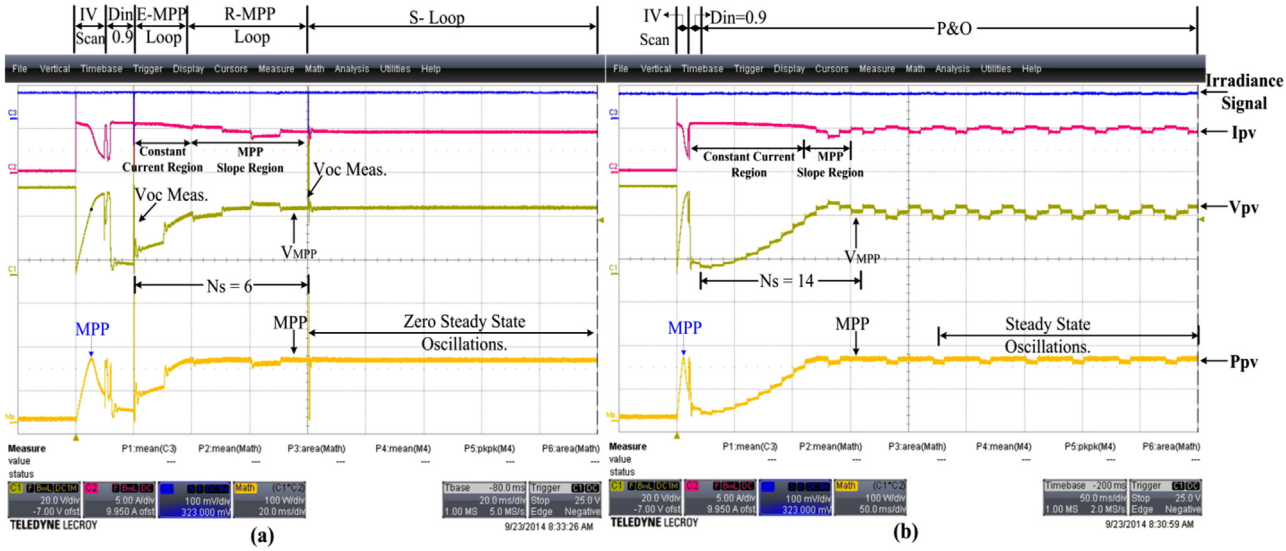

Fig. 14. Performance of techniques at medium irradiance against resistive load.

Table 2
Implementation cost and embedded system of MPPTs.

Techniques	Complex operations	Embedded system				Sensors	Extra circuits	Implementation cost
		Processing unit	Processing speed	Data acquisition unit				
				Frequency	Resolution			
ProposedMPPT	Exponential, square root, division	Advanced	Low microseconds	Moderate	Moderate	V_{pv}, I_{pv}	V_{oc}—Switch	Middle
Sliding [3]	Tangent, division	Advanced	High nanoseconds to low microseconds	High	High	V_{pv}, I_L	I_{pv}—Sallen-key filter	Highest
MPPT [31]	Square root, division, low-point fractions	Advanced	Low microseconds	Moderate	High	V_{pv}, I_{pv}	–	Middle
P&O	–	Basic	Low microseconds	Moderate	Moderate	V_{pv}, I_{pv}	–	Lowest

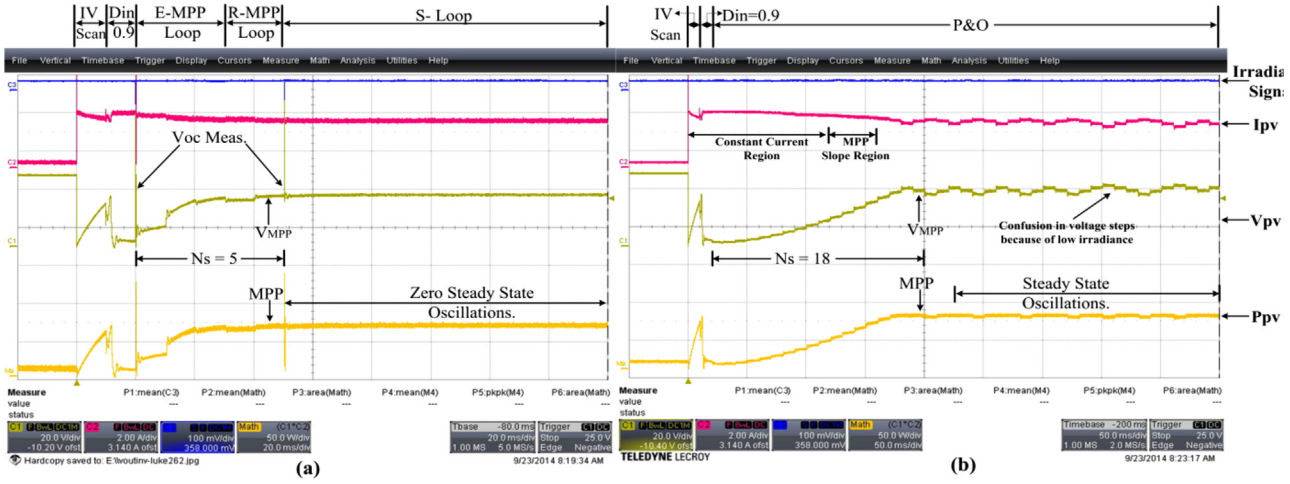

Fig. 15. Response of techniques at low irradiance against resistive load.

Table 3
Time response of techniques under distinct weather conditions.

Load	Proposed MPPT						P&O					
	Weather conditions		V_{mpp} (V)	D_{mpp}	N_s	T_r	Weather conditions		V_{mpp} (V)	D_{mpp}	N_s	T_r
	I_{sc}	Irradiance					I_{sc}	Irradiance				
Resistive (47 Ω)	9.93 A	High	25.78	0.757	5	50 ms	9.81 A	High	26.79	0.78	9	90 ms
	5.74 A	Medium	29.08	0.635	6	60 ms	5.60 A	Medium	29.46	0.66	14	140 ms
	2.89 A	Low	27.6	0.496	5	50 ms	2.87 A	Low	27.58	0.48	18	180 ms
Battery (49.1 V)	9.13 A	High	26.39	0.505	9	90 ms	9.01 A	High	27.91	0.48	18	180 ms
	2.65 A	Low	27.82	0.463	10	100 ms	2.76 A	Low	29.6	0.42	20	200 ms

irradiance is 30% (High: 0.78 (78%)–Low: 0.48 (48%)) while the difference in V_{mpp} values between the two is merely 0.79 V (High: 26.79 V–Low: 27.58 V). It should be noted that initial D_{in} is set at 0.9 (90%), both techniques have to cross the constant current region in order to reach the MPP region. Since D_{mpp} values continue to move away from D_{in} = 0.9 as the conditions falls, which can be seen from Table 3, P&O spends more time in the constant current region before reaching the MPP region because of its one-dimensional approach. On the other hand, the proposed technique estimates the V_{mpp} and skips the constant current region courtesy E-MPP loop and executes almost similar samples in each and every condition.

6.1.2. Battery load (49.1 V)

Figs. 16 and 17 show the response of two techniques at high and low irradiance levels respectively against the battery load. On both occasions, the proposed technique exhibits better performance as it takes half samples to search the MPP compared to P&O. Note that the P&O performance does not degrade significantly while moving from high to low irradiance condition as it takes 2 more samples at low irradiance compared to high irradiance. It is because that under battery load, the D_{mpp} is not significantly changed with the change in irradiance as indicated in Table 3.

6.1.3. Summary

Table. 3 clarifies that since the S_R of both technique is set at 10 ms, the worst response time T_r (calculated from Eq. (21)) for the proposed technique to reach MPP is 100 ms. While the worst T_r for the P&O is double i.e. 200 ms. Thus, the proposed technique outperforms the P&O by a significant margin.

6.2. Dynamic and steady state response of techniques

Figs. 18 and 19 show the dynamic response of two techniques under the resistive load. To conduct this test, the time resolution of digital oscilloscope is set at 5 s/div such that 50 s of real time data can be recorded and then following steps are executed: (1) PV array is placed facing the sun and the techniques are allowed to settle at MPP under the present weather condition, (2) PV array

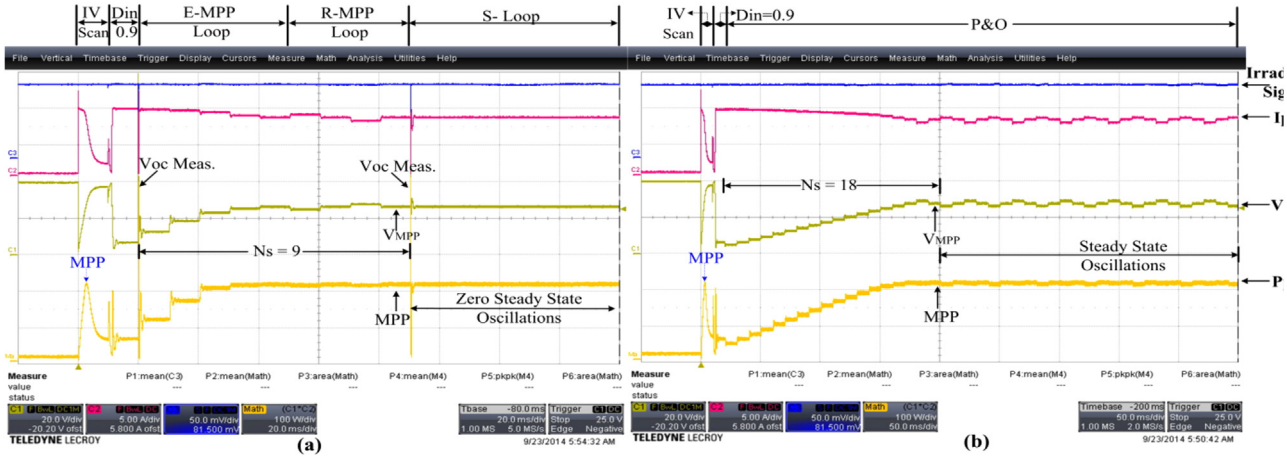

Fig. 16. Operation of techniques at high irradiance against battery load.

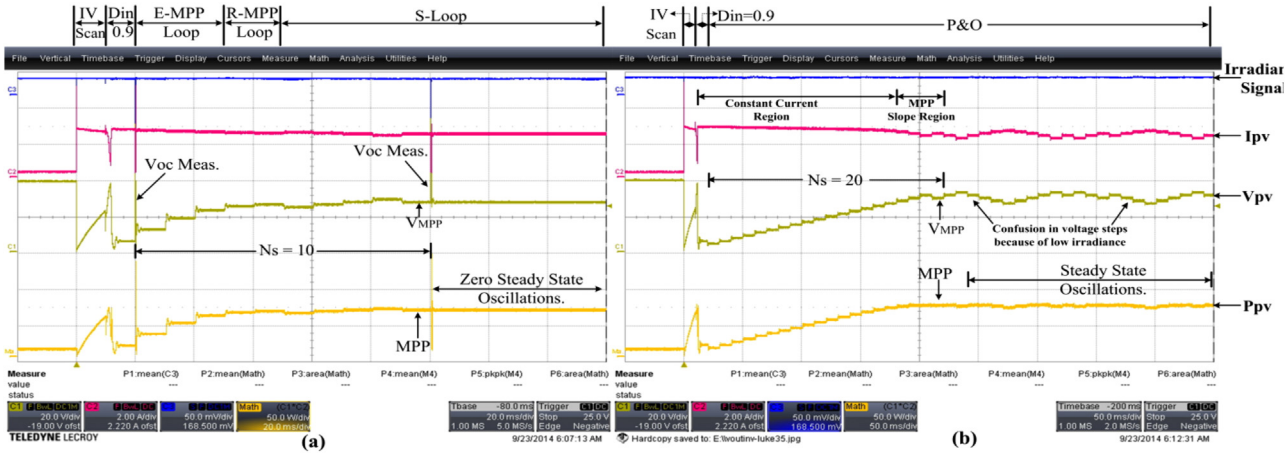

Fig. 17. Performance of techniques at low irradiance against battery load.

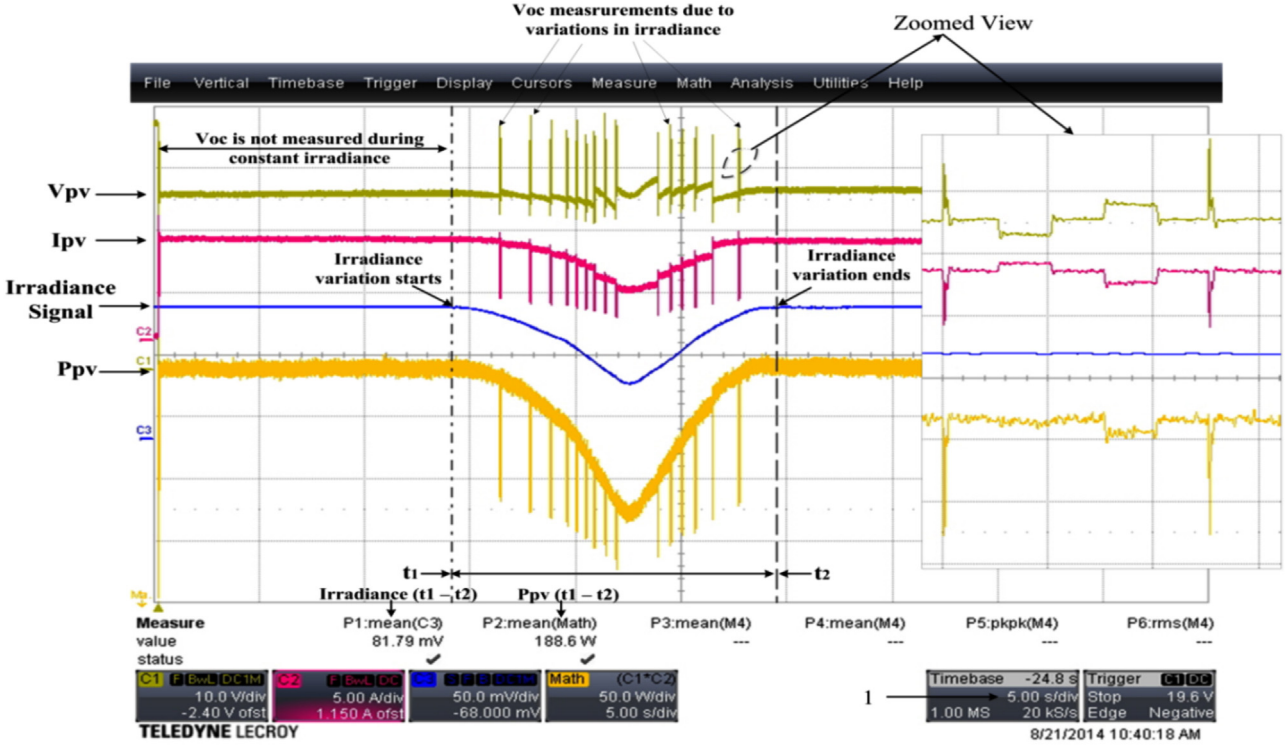

Fig. 18. Dynamic response of proposed MPPT under varying weather conditions.

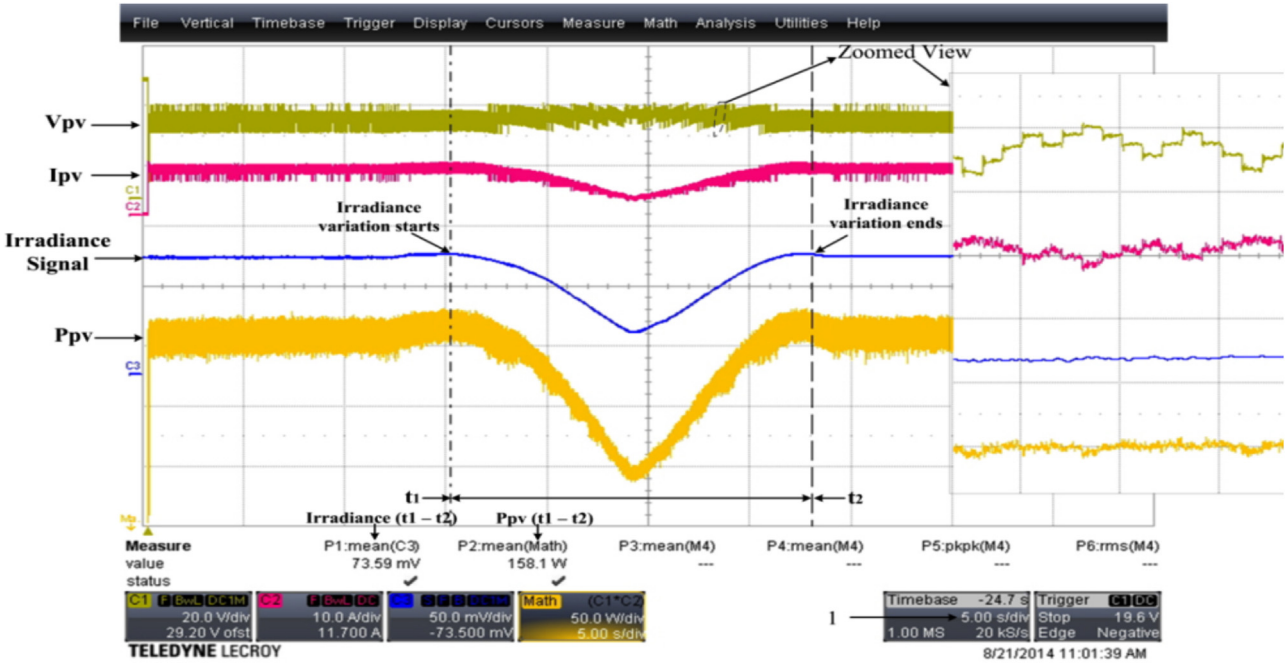

Fig. 19. Dynamic response of P&O under varying weather conditions.

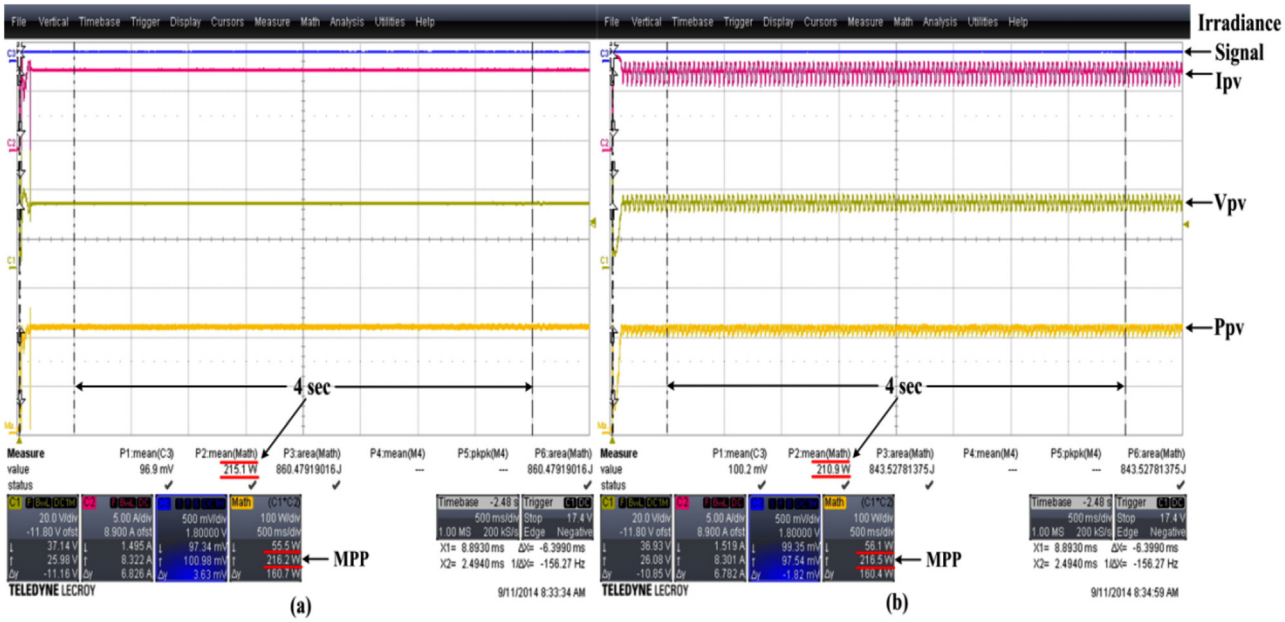

Fig. 20. Steady state response of techniques against resistive load.

is moved clockwise (away from the sun) with the help of mobile vehicle, which is indicated by the "Irradiance variation starts" in Figs. 18 and 19, (3) PV array is moved anti-clockwise (towards the sun) and stopped at the point indicated by "Irradiance variation ends" and (4) dynamic efficiency of the technique is measured with the help of Eq. (23) [32], from the time (t1) when the irradiance starts to change to the time (t2) when irradiance variation ends. Both t1 and t2 are indicated in Figs. 18 and 19. In Eq. (23), P_{MPPT} is the cumulative power of the technique while P_{Ideal} is the ideal power, which is calculated with the help of irradiance signal.

$$\eta_{MPPT} = \frac{\int_{t1}^{t2} P_{MPPT}(t)\,dt}{\int_{t1}^{t2} P_{Ideal}(t)dt} \tag{23}$$

Fig. 18 shows that the P_{pv} of the array follows the irradiation signal with the aid of the proposed technique, which indicates that PV array captures the MPP line effectively. P_{pv} of array shows the spikes at different instants indicating the V_{oc} measurements. A zoomed view of one of the V_{oc} measurement instant along with the process of the proposed technique is also shown on the right side. Fig. 19 depicts the dynamic response of P&O, which indicates that P&O struggles to focus the MPP line with the same efficiency as that of the proposed MPPT. One of the iteration of P&O is shown in zoomed view on the right side of Fig. 19.

On the other hand, Figs. 20 and 21 demonstrate the steady response of both techniques under resistive and battery loads respectively. It can be seen that P&O exhibits power loss oscilla-

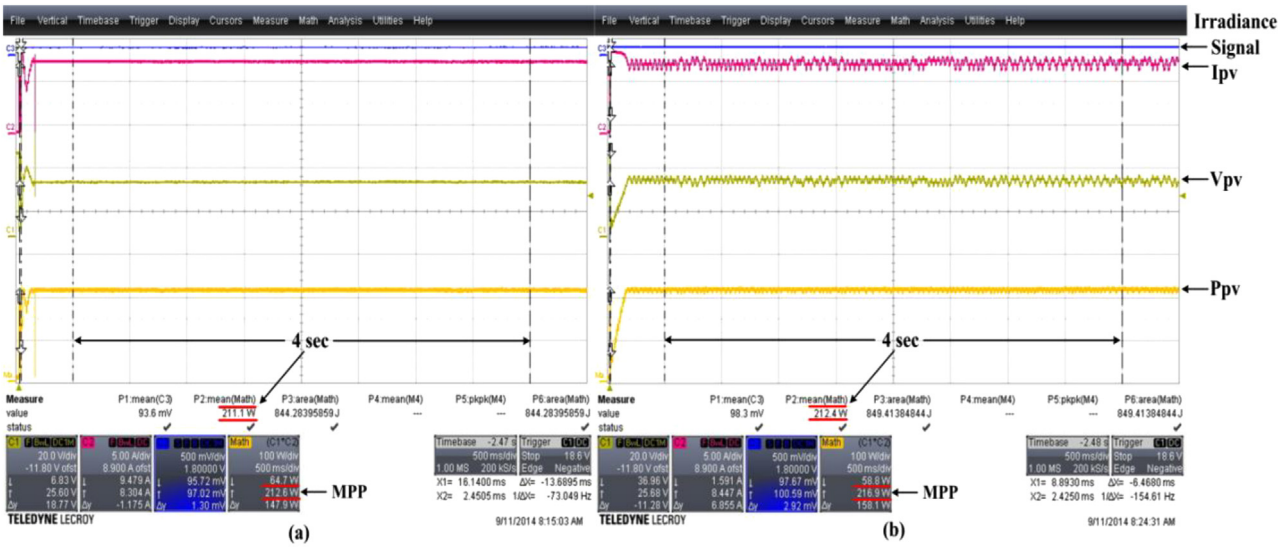

Fig. 21. Steady state response of techniques against battery load.

Table 4
Experimental dynamic and steady efficiencies of the proposed MPPT & P&O.

Weather conditions	Load type		Efficiency (η_{MPPT})	
	Type	Value	Proposed MPPT	P&O
Dynamic	Resistive	47 Ω	97.3%	90.8%
Steady	Resistive	47 Ω	99.5%	97.4%
Steady	Battery	49.1 V	99.3%	97.9%

tions around MPP as shown in Figs. 20 (b) and 21 (b), while the proposed technique is stable at MPP in its S-loop as illustrated by Figs. 20 (a) and 21 (a).

Table 4 indicates that the proposed technique has a dynamic efficiency of 97.3%, which is almost 6.5% superior than the efficiency of P&O. Thus justifying the time response analysis discussed in the previous section that P&O requires more samples to reach MPP compared to proposed MPPT. Similarly, the steady state efficiency of the proposed MPPT hovers around 99.5%, which is almost 2% more efficient than P&O steady state efficiency under both kinds of loads.

7. Conclusions

In this paper, a new hybrid MPPT technique has been proposed to optimize the perturb and observe technique. The followings are the highlights of the proposed work: (1) duration of V_{oc} measurement has been figured out, (2) relations have been developed which provide estimations of V_{mpp}, I_{mpp} & D_{mpp}, (3) in order to judge the varying weather conditions, the frequency of V_{oc} measurement is set and then criterion is formulated with respect to the sampling rate of PV system and (4) limits criteria is developed to judge the steady weather conditions.

All these features are embedded into the control architecture of proposed technique, which makes it less complex compared to past proposed MPPTs, and yet exhibits better performance. The effectiveness of the MPPTs has been carried out using the computer aided simulations and experimental setup. It has been verified through the comparative analysis that the proposed MPPT has superior performance than the other technique in terms of dynamic and steady state efficiencies.

References

[1] D. Veram, S. Nema, A.M. Shandilya, S.K. Dash, Maximum power point tracking (MPPT) techniques: recapitulation in solar photovoltaic systems, Renew. Sustain. Energy Rev. 54 (2016) 1018–1034.
[2] Y. Hong, S.N. Pham, T. Yoo, K. Chae, K.-H. Baek, Y.S. Kim, Efficient maximum power point tracking for a distributed PV system under rapidly changing environmental conditions, IEEE Trans. Power Electron. 30 (March (8)) (2015) 4209–4218.
[3] D.G. Montoya, C.A.R. Paja, R. Giral, Maximum power point tracking of photovoltaic systems based on the sliding mode control of the module admittance, Electr. Power Syst. Res. 136 (2016) 125–134.
[4] F. Spertino, J. Ahmad, A. Ciocia, P.D. Leo, A.F. Murtaza, M. Chiaberge, Capacitor charging method for I–V curve tracer and MPPT in photovoltaic systems, Sol. Energy 119 (2015) 461–473.
[5] M. Carrasco, F. Mancilla-David, Maximum power point tracking algorithms for single-stage photovoltaic power plants under time-varying reactive power injection, Sol. Energy (2016) 321–331.
[6] P.K. Peter, V. Agarwal, On the input resistance of a reconfigurable switched capacitor DC–DC converter-based maximum power point tracker of a photovoltaic source, IEEE Trans. Power Electron. 27 (December (12)) (2012) 4880–4893.
[7] P.K. Peter, V. Agarwal, Maximum power point tracking scheme for PV systems operating under partially shaded conditions, IEEE Trans. Power Electron. 55 (April (4)) (2008) 1689–1698.
[8] T. Esram, P.L. Chapman, Comparison of photovoltaic array maximum power point tracking techniques, IEEE Trans. Energy Convers. 22 (June (2)) (2007) 439–1698.
[9] Z. Salam, J. Ahmed, B.S. Merugu, The application of soft computing methods for MPPT of PV system: a technological and status review, Appl. Energy 107 (2013) 135–148.
[10] C.-S. Chiu, T-S fuzzy maximum power point tracking control of solar power generation systems, IEEE Trans. Energy Convers. 25 (December (4)) (2010) 1123–1132.
[11] T.L. Kottas, Y.S. Boutalis, A.D. Karlis, New maximum power point tracker for PV arrays using fuzzy controller in close cooperation with fuzzy cognitive networks, IEEE Trans. Energy Convers. 21 (September (3)) (2006) 793–1132.
[12] J.J. Soon, K.-S. Low, Photovoltaic model identification using particle swarm optimization with inverse barrier constraint, IEEE Trans. Power Electron. 27 (September (9)) (2012) 3975–3983.
[13] K. Ishaque, Z. Salam, G. Lauss, The performance of perturb and observe and incremental conductance maximum power point tracking method under dynamic weather conditions, Appl. Energy 119 (2014) 228–236.
[14] A. Murtaza, M. Chiaberge, M. De-Giuseppe, D. Boero, A duty cycle optimization based hybrid maximum power point tracking technique for photovoltaic systems, Electr. Power Energy Syst. 59 (2014) 141–154.
[15] D.P. Hohm, M.E. Ropp, Comparative study of maximum power point tracking algorithms, Prog. Photovoltaics: Res. Appl. 11 (2003) 47–62.
[16] E. Bianconi, J. Calvente, R. Giral, E. Mamarelis, G. Petrone, C.A. Ramos-Paja, G. Spagnuolo, M. Vitelli, Perturb and observe MPPT algorithm with a current controller based on the sliding mode, Int. J. Electr. Power Energy Syst. 44 (2013) 346–356.
[17] A.M.Z. Alabedin, E.F. El-Saadany, M.M.A. Salama, Maximum power point tracking for photovoltaic systems using fuzzy logic and artificial neural networks, IEEE Power Energy Soc. Gen. Meet. (2011) 1–9.
[18] A.K. Abdelsalam, A.M. Massoud, S. Ahmed, P.N. Enjeti, High-performance adaptive perturb and observe MPPT technique for photovoltaic-based microgrids, IEEE Trans. Power Electron. 26 (April (4)) (2011) 1010–1021.

[19] J.S.C.M. Raj, A.E. Jeyakumar, A novel maximum power point tracking technique for photovoltaic module based on power plane analysis of I–V characteristics, IEEE Trans. Ind. Electron. 61 (September (9)) (2014) 4734–4745.
[20] F. Zhang, K. Thanapalan, A. Procter, S. Carr, J. Maddy, Adaptive hybrid maximum power point tracking method for a photovoltaic system, IEEE Trans. Energy Convers. 28 (June (2)) (2013) 353–360.
[21] T. Tafticht, K. Agbossou, M.L. Doumbia, A. Cheíriti, An improved maximum power point tracking method for photovoltaic systems, Renew. Energy 33 (2007) 1508–1516.
[22] M.H. Moradi, A.R. Reisi, A hybrid maximum power point tracking method for photovoltaic systems, Sol. Energy 85 (2011) 2965–2976.
[23] P.A. Ortiz-Valencia, C.A. Ramos-Paja, Sliding-mode controller for maximum power point tracking in grid-connected photovoltaic systems, Energies 8 (11) (2015) 12363–12387.
[24] M.R. Mojallizadeh, M.A. Badamchizadeh, S. Khanmohammadi, M. Sabahi, Designing a new robust sliding mode controller for maximum power point tracking of photovoltaic cells, Sol. Energy 132 (2016) 538–546.
[25] http://www.kyocera.com.sg/products/solar/pdf/kc200gt.pdf (Accessed January 2017).
[26] M.G. Villalva, J.R. Gazoli, E.R. Filho, Comprehensive approach to modeling and simulation of photovoltaic arrays, IEEE Trans. Power Electron. 24 (May (5)) (2009) 1198–1208.
[27] F. Spertino, J. Sumaili, H. Andrei, G. Chicco, PV module parameter characterization from the transient charge of an external capacitor, IEEE J. Photovoltaics 3 (October (4)) (2013) 1325–1333.
[28] J. Qi, Y. Zhang, Y. Chen, Modeling and maximum power point tracking (MPPT) method for PV array under partial shaded conditions, Renew. Energy 66 (2014) 337–345.
[29] A.M. Latham, R. Pilawa-Podgurski, K.M. Odame, C.R. Sullivan, Analysis and optimization of maximum power point tracking algorithms in the presence of noise, IEEE Trans. Power Electron. 28 (July (7)) (2013) 3479–3494.
[30] N. Femia, G. Petrone, G. Spagnuolo, M. Vitelli, Optimization of perturb and observe maximum power point tracking method, IEEE Trans. Power Electron. 20 (July (4)) (2005) 963–973.
[31] K.S. Tey, S. Mekhilef, A fast-converging MPPT technique for photovoltaic system under fast varying solar irradiation and load resistance, IEEE Trans. Energy Convers. 11 (February (1)) (2015) 176–186.
[32] S. Daraban, D. Petreus, C. Morel, A novel MPPT (maximum power point tracking) algorithm based on a modified genetic algorithm specialized on tracking the global maximum power point in photovoltaic systems affected by partial shading, Energy 74 (2014) 374–388.